Equatorial wave diagnosis for the Atlantic Niño in 2019 with an ocean reanalysis.

Qingyang Song[1,2] and Hidenori Aiki[3]

[1]Key Laboratory of Marine Hazards Forecasting, Ministry of Natural Resources, Hohai University, Nanjing, China
[2]College of Oceanography, Hohai University, Nanjing, China
[3]Institute for Space-Earth Environmental Research, Nagoya University, Nagoya, Japan

Correspondence: Qingyang Song (qysong@hhu.edu.cn)

Abstract. The propagation of equatorial waves is essential for the onset of Atlantic Niño, but diagnosing waves using ocean reanalysis or in-situ data remains a challenge. This study uses an ocean reanalysis to diagnose the wave energy transfer route during the 2019 event. The climatological values and the anomaly in 2019 at each grid are decomposed into the first four baroclinic modes based on their local density profiles. The decomposed geopotential can well reproduce the displacement of the thermocline during the event. Wave energy flux is calculated by means of a group-velocity-based scheme. In addition to detecting wind-forced Kelvin waves and reflected Rossby waves, the wave energy flux reveals another possible energy transfer routes along the western boundary, where some off-equatorial wave energy can excite coastally-trapped Kelvin waves and transfer back to the equatorial Atlantic. Four transections are selected, and the passing wave energy fluxes for 2019 are integrated across them. The results suggest that the Kelvin waves in the third and fourth mode are local forced, while the wave energy in the second mode is more likely from the off-equatorial region. Therefore, in the fall of 2019, the second-mode Kelvin waves causes the thermocline to drop ahead of other modes from September, serving to precondition the Niño event.

1 Introduction

The equatorial Atlantic Ocean is known for exhibiting pronounced anomalies of sea surface temperature (SST) on interannual time scales, often referred to as the Atlantic Niño. This phenomenon is essentially driven by the Bjerknes feedback, that the westerly wind anomaly caused by the SST anomaly in the east equatorial basin excites equatorial waves and consequently amplifies the SST anomaly through thermocline displacement due to the wave propagation. The impact of these SST events is not limited to affecting precipitation and monsoon patterns in the surrounding sea area and continent, but also extends to the Pacific and Indian Oceans through atmospheric teleconnections (Carton et al., 1996; Okumura and Xie, 2004; Foltz et al., 2019; Lübbecke and McPhaden, 2012).

Since 2000, the interannual variability of SST has been revealed to become weaker (Tokinaga and Xie, 2011; Crespo et al., 2022). Although the cause to suppress the Atlantic Niño events remains unclear, the thermal dynamic rather than the oceanic dynamic was previously thought to play a critical role in the decline trend (Nnamchi et al., 2015; Crespo et al., 2022). A warmer climate deepens the upper ocean layer making it less sensitive to upwelling anomalies (Crespo et al., 2022). That is, different from the equatorial Pacific, where the changes in the zonal SST gradient under greenhouse forcing are most relevant (Latif

25   and Keenlyside, 2009), a basin-wide warming associated with the climate change can eventually break the classic Bjerknes loop so as to limit the development of SST anomaly. Despite the predicted long-term weakening trend for SST variability, two extremely warm SST events occurred in the winter of 2019 and the second half of 2021. As a result, a warning system is still necessary in the short term.

Evidences were reported that the Atlantic Niño events in both 2019 and 2021 are strongly related with off-equatorial Rossby
30   waves (RW) in (Richter et al., 2022). The equatorial Atlantic basin is narrow and has an inwardly-tilted coastline in the north-east. This allows waves from off-equatorial regions to travel through the basin quickly and also results in more wave energy being directed back towards the equatorial sector. When the off-equatorial RWs approach the western boundary, reflected Kelvin waves (KW) are excited and consequently displace the thermocline to affect SST in the equatorial Atlantic (Foltz and McPhaden, 2010). This dynamic link suggests that the wave condition is still crucial for the prediction of the Niño events
35   at this moment. Indeed, researchers have already proposed to use equatorial waves to warn the anomalous SST event in the down-wave coastal region (Imbol Koungue et al., 2017, 2019; Illig and Bachèlery, 2019). The period that wave energy transfers horizontally and vertically (normally takes several months to pass the basin depending on the baroclinic mode and around one month up to the sea surface) from the west of the equatorial Atlantic or further from the off-equatorial region gives the equatorial wave the potential to be a effective predictor for the Atlantic Niño at its onset stage.

40   For establishing an early warning system, Imbol Koungue et al. (2017, 2019); Song et al. (2023) suggested to implement ocean linear model in real time that simulates equatorial waves in addition to involve in-situ and altimetric data. The implementation of ocean linear model in those proposals are necessary, as the energy from RWs in off-equatorial region are previously difficult to diagnose with observed or modelled data (Rossby, 1945; Philander, 1978; Schopf et al., 1981; Schiller et al., 2010). However, benefiting from a newly unified wave energy flux schemes for equatorial waves by Aiki et al. (2017),
45   which they named as AGC flux (standing for the authors, Aiki, Greatbatch and Claus), the wave energy flux that are transferred in the tropical Atlantic Ocean can be diagnosed by only applying dataset of current velocity and pressure (Song and Aiki, 2020, 2021). Currently the high-resolution dataset (eg. 1/12° horizontal resolution and 50 vertical levels provided by Copernicus Marine Environment Monitoring Service) is available to capture the rapid gravity waves such as KWs in low baroclinic mode (Jean-Michel et al., 2021); Also, Prediction and Research Moored Array in the Tropical Atlantic (PIRATA) initiated in
50   1997 can provide real time in-situ observation in the tropical Atlantic (Bourlès et al., 2019). These datasets offer an opportunity to develop a wave warning system that does not require a linear ocean model, provided that wave energy from both the off-equatorial and equatorial regions can be evaluated during the event year. This study is an attempt of applying the AGC flux in an ocean reanalysis to assess wave energy in the event year 2019. We hope that our investigation for the process of the wave energy transfer and its impact on the Atlantic Niño can inspire a simple and reliable system to predict anomalous SST events
55   through diagnosing existing dataset.

The structure of this manuscript is as follows: Section 2 briefly explains the applied dataset and the method to extract the wave information from the data; In Section 3 we present the decomposed waves and construct the wave energy transfer route (the trajectory of wave energy transport) in 2019, which we compare with the climatological data to evaluate the extraordinary

wave energy from both the equatorial and the off-equatorial region during the Niño event; Section 4 summarizes the addressed

60   problems and conclusions of this study.

2   Wave detection with reanalysis data

The reanalysis dataset we employed in this study is the GLORYS12V1 product from CMEMS (Copernicus Marine Envi-
ronment Monitoring Service). The product is a global ocean eddy-resolving (1/12° horizontal resolution, 50 vertical levels)
reanalysis using reduced-order Kalman filter and 3D-VAR scheme to involve along track altimeter data, satellite SST, sea ice

65   concentration and in-situ temperature and salinity vertical profiles in joint assimilation (Jean-Michel et al., 2021). The product
provides daily and monthly dataset including potential temperature, salinity, current velocity, mixed-layer thickness and sea
surface height (SSH) covering the altimetry (1993 onward). Daily data are used to detect the equatorial waves in the event year;
monthly data are applied to obtain climatology and mean ocean state.

The decomposition of baroclinic waves from the ocean reanalysis requires the solution of the eigen equation in the vertical

70   direction as follows,

$$
\frac{\partial}{\partial z}\left(\frac{1}{N^2}\frac{\partial \psi^{(n)}}{\partial z}\right) = -\frac{1}{(c^{(n)})^2}\psi^{(n)}, \tag{1}
$$

which subject to the boundary conditions $\psi_z^{(n)}(0) = \psi^{(n)}(-H_b) = 0$. The symbol H_b is the ocean bottom depth, N is the
Brunt-Väisälä frequency estimated by the mean vertical profiles of temperature and salinity, and $\psi^{(n)}$ is the eigen function of
the nth baroclinic modes for the corresponding gravity wave speed (eigen value) $c^{(n)}$. Then based on the linear theory, the

75   wave-induced anomaly subjects to

$$
\begin{aligned}
u'(x,y,z,t) &= \sum u^{(n)}(x,y,t)\psi^{(n)}(z), \\
v'(x,y,z,t) &= \sum v^{(n)}(x,y,t)\psi^{(n)}(z), \\
p'(x,y,z,t) &= \sum p^{(n)}(x,y,t)\psi^{(n)}(z),
\end{aligned} \tag{2}
$$

where (u',v') is the anomaly of velocity component and p' is the geopotential anomaly, representing the displacement of
gravity potential by both the density anomaly and the volume transport as follows,

$$
p' = g\eta(x,y,t) + \frac{g}{\rho_0}\int_z^0 \rho'(x,y,z,t)\mathrm{d}z, \tag{3}
$$

80   where η is the sea level anomaly and ρ' is the density anomaly. To decompose the wave, following Toyoda et al. (2021), we
integrate both side of Eq. (2) in the vertical direction after multiplying $\psi^{(n)}$. Utilizing the orthogonality of the eigen function,

we have

$$u^{(n)} = \left[\int_{-H_b}^{0} u'\psi^{(n)}\mathrm{d}z\right]\left[\int_{-H_b}^{0} (\psi^{(n)})^2\mathrm{d}z\right]^{-1},$$

$$v^{(n)} = \left[\int_{-H_b}^{0} v'\psi^{(n)}\mathrm{d}z\right]\left[\int_{-H_b}^{0} (\psi^{(n)})^2\mathrm{d}z\right]^{-1},$$

$$p^{(n)} = \left[\int_{-H_b}^{0} p'\psi^{(n)}\mathrm{d}z\right]\left[\int_{-H_b}^{0} (\psi^{(n)})^2\mathrm{d}z\right]^{-1}. \tag{4}$$

Thus, by substituting the (u', v') and p' obtained from the daily reanalysis data and the $\psi^{(n)}$ solved from Eq (1) to Eq (4),
wave-induced anomalies in the corresponding baroclinic modes are extracted. In this study, $c^{(n)}$ and $\psi^{(n)}$ are solved using N
estimated by the mean vertical profiles of temperature and salinity data from 1993 to 2020 of the monthly reanalysis product.
Although the yielded $\psi^{(n)}$ and $c^{(n)}$ are spatially varying (see Figure 1 and Figure 2), the $\psi^{(n)}$ in the above decomposition
process is decoupled from the horizontal motions, given that the wave energy exchange between baroclinic modes is depressed
during the wave propagation. Thus, the $\boldsymbol{V}^{(n)} = (u^{(n)}, v^{(n)})$ and $p^{(n)}$ are conserved in each mode, which makes the application
of AGC scheme possible to detect equatorial waves by diagnosing the wave energy flux in the corresponding mode. Here we
utilize the AGC level2 scheme by Aiki et al. (2017) as follows,

$$\boldsymbol{c_g}\overline{E} \approx \overline{\boldsymbol{V}^{(n)}p^{(n)}} + \nabla \times \overline{(p^{(n)}(\varphi^{(n)})}/2)\boldsymbol{z}, \tag{5}$$

where $E^{(n)} = \frac{1}{2}[(u^{(n)})^2 + (v^{(n)})^2 + (p^{(n)}/c^{(n)})^2]$ is the sum of kinetic and gravitational energies and $\boldsymbol{c_g}$ is the group velocity.
The overline symbol in Eq. (5) is a phase average operator provided by Aiki et al. (2017). $\nabla \times \overline{(p^{(n)}(\varphi^{(n)})}/2)\boldsymbol{z}$ is a offset term,
which includes a scalar quantity $\varphi^{(n)}$ solved by

$$\Delta\varphi^{(n)} - (f/c^{(n)})^2\varphi^{(n)} = q^{(n)}, \tag{6}$$

where $q^{(n)} = \frac{\partial v^{(n)}}{\partial x} - \frac{\partial u^{(n)}}{\partial y} - \frac{p^{(n)}f}{(c^{(n)})^2}$ is the Ertel's potential vorticity (EPV). Then though Eq. (5), pressure flux is redirected
to the direction of group velocity. The equatorial waves including KW, RW and even the mixed RW (Yanai wave) in the event
year 2019 are hence able to be detected from the reanalysis data by analysing the wave energy flux.

Equatorial waves are subject to linear shallow water equation (Matsuno, 1966), which are mainly forced by atmospheric
forcing and some baroclinic instability. Due to the resonance mechanism, we can expect that waves will be more easily gener-
ated by forcing with the period that is close to the basin-mode period (defined as the four times of the period for KW to travel
through the whole equatorial basin). Here since the wave-induced anomaly in the event year 2019 as well as the climatology
are focused, we will direct our analysis towards the first four gravest baroclinic modes, whose basin-mode periods (based on
the average gravity wave speed) are no longer than 1.5 years. It should be pointed out here that, as waves in each baroclinic
mode are already decoupled by Eq. (4), the selection of modes for the decomposition will not affect the decomposition result.

3 Results

3.1 Wave-induced variability

The extracted wave signal from the climatological data include both the wind-forced waves and the instability waves. In
110 agreement with previous results from linear model that are driven by the climatological forcing (Song and Aiki, 2020), the
obtained variability of $u^{(n)}$ and $p^{(n)}$ at the equator are revealed largely in annual and semi-annual periods (see Figure 3). In
the western basin, annual signals of both zonal velocity and geopotential are both notable for the four modes. However, from
around $15°$W, the signals become nearly semi-annual (see Figure 3). The two peaks of both zonal velocity and geopotential
in the central and eastern basin should be owing to the mixture of two waveguides that the one originated from the central
115 basin in May merges with the other from western basin in Sep. (Song and Aiki, 2020; Ding et al., 2009). The magnitude of
the zonal velocity anomaly in each mode is also significantly influenced by the basin-mode period. Specifically, the annual or
semi-annual variability of zonal velocity becomes stronger when the period calculated by the averaged wave speed is closer to
one or half a year (Song and Aiki, 2020; Claus et al., 2016). Thus the zonal velocity anomaly in the second, third and fourth
mode are all found prominent in Figure 3 c, e & g. It should be also noted that in the presence of thermal-induced seasonal
120 variability in sea temperature and salinity, despite the first-mode zonal velocity is relatively weak, its geopotential anomaly is
still prominent (Figure 3 a & b).

We further investigate the wave-induced anomaly in 2019 to determine the feature of waves during the event. Figure 4
confirms that, after removing the climatological values, the decomposed geopotential anomalies for the first four modes is able
to reproduce the thermocline drop for the 2019 winter event which is around one month ahead of the SST rising. The extracted
125 waves in 2019 have demonstrated prominent variability of meridional velocity in all the presented modes with sign-alternating
distributions along the equator (see Figure 5). It may suggest that mixed RWs in the nature of cross equatorial meridional
velocity are raised by subseasonal forcing. The subseasonal forcing can excite KWs or inertial waves as well to enhance the
variability of zonal velocity especially in the first mode due to its faster gravity wave speed (see Figure 5 a). In the other
three mode, the travelling signals of zonal velocity (see Figure 5 are also prominent and some of them do not present notable
130 propagation patterns (e.g. the second and the fourth modes) as the climatological scenario. Correspondingly, Figure 5 b, d, f & h
have suggested that from the fall of 2019, there are positive geopotential anomalies in all the four modes jointly causing the
drop of the thermocline. Those facts may indicate the additional KW trains induced by the subseasonal forcing that causes
the negative displacement of thermocline thereby triggering the Atlantic Niño in 2019. Certainly, as the meridional velocity
anomaly is notable, the influence by waves from off-equatorial region is also expected.

3.2 Horizontal wave energy flux

As the group velocity can be used to identify KWs and RWs, we first investigate the horizontal distribution of annual mean zonal
wave flux (Figure 6 and Figure 7), which can effectively indicate the dominant location and type of waves in each baroclinic
mode. In the climatological scenario (Figure 6), the AGC level2 scheme manifests clear equatorial KW trains originated from
the western Atlantic basin transporting the energy to the eastern boundary where it excites the reflected RWs and bring the

140   energy back to the west. With the decrease of Rossby deformation radius, wave energy in high baroclinic modes tends to limit in a narrow latitude range. It is strong eastward energy flux in the first mode (see Figure 6 a) that has not been seen in the research by Song and Aiki (2020) with linear ocean models. The flux is due to the along-shore waves off the western boundary that bring the energy to the equatorial Atlantic from the extra-tropical region. Indeed, the planetary basin mode leads to the wave cycle that the coastally-trapped KW from high latitude will travel back to the equatorial region (Yang and Liu,

145   2003). Nevertheless this coastally-trapped KW can not be well reproduced in linear models because they usually apply radiant boundaries in both north and south rather than using enclosed basins as the real Atlantic Ocean (Matsuno, 1966; Song and Aiki, 2020). In the event year 2019, the annual mean wave flux for the subseasonal waves at the equator to transport the energy eastward is also prominent. Even in the second and third baroclinic modes, both the eastward wave flux in the off-equatorial region and the westward wave flux in the western basin exhibit greater strength than the climatological values in Figure 6. This

150   result may suggest that the onset of the Atlantic Niño is associated with strong KWs induced by both subseasonal local forcing and off-equatorial energy.

We then investigate the evolution of wave energy flux at the equator in 2019. In Figure 8, by comparing the theoretical group velocity of KWs and RWs (solid red and blue) in corresponding modes, subseasonal waveguides can be detected. There are multiple KW trains passing through the basin in 2019. For all the four modes, strong KWs are excited in spring (from

155   around Apr.) and fall (from around Sep.) keep transferring the energy for several month depending on their wave periods and group velocities. Most of the KWs are originated from the western basin but some of them are notably strengthened in the central and eastern basin (e.g. in around Dec. for the first mode as Figure 8 a and for the third mode as Figure 8 c). However, KW trains do not guarantee the drop of thermocline, the superposition of out-of-phase geopotential by waves in multiple modes may eliminate the displacement (Song et al., 2023). In the fall and winter, we do find the positive geopotential anomaly

160   (representing the drop of thermocline to induce the positive SST anomaly) in the four modes (see Figure 5). In the spring and summer, nevertheless, the second and fourth mode are dominated by the the negative geopotential anomaly which is likely eliminate the positive anomaly in the first and third mode so as to prevent the occur of the event in this season (see Figure 5). It may suggest that the KWs in the four modes with different phases of geopotential anomaly are not all excited by the local wind. Other energy sources should be taken into account, e.g. the RW trains (see solid blue line and blue contours) are indicating the

165   possibility of reflected KWs to be excited in fall. Multiple energy sources may cause the diversity of geopotential phase.

3.3   Wave energy transfer process

In this section, we integrate the energy flux over several meridional transections to further investigate the wave energy transfer process in 2019. As shown by the solid yellow lines in Figure 7, we have selected three sections (S2-S4) in the equatorial region with the length of six degree (3°S-3°N) to match the recognized boundary of western Atlantic basin (40°W-20°W) and

170   the ATL3, 20°W-0°), and an off-equatorial section (S1) ($45°W$,4°N-10°N) to capture the westward energy flux (see Figure 7) that may approach the western boundary and transfer energy back to the equatorial region.

The variances of the wave energy flux passing through the four selected transections in 2019 are presented in Figure 9. Although the prominence of the eastward wave energy flux has been illustrated in all the four baroclinic modes at the onset

stage of the SST event from around Oct. (see Figure 9), it is noteworthy that there is diversity among modes in transections
with the largest passing energy flux . The third and fourth modes are both found to have the largest eastward energy flux to
pass S4 but the energy flux passing S1, S2 and S3 are all weak. This may suggest that the waves in the two modes are local
forced in the ATL3 region. So that the energy source is located between S3 and S4 to excite the KW tranferring the energy east
through S4 (see solid red line in Figure 9 c & d). Meanwhile it may also excite RW to westward pass S3 (see solid blue line in
Figure 9 c). Correspondingly, the eastward energy flux passing S3 for both the first and the second modes is found to be strong,
which suggests the KWs that are forced in the west of the ATL3. Moreover, in the second mode, the westward energy flux at
S1 peaks in around Sep. and subsequently, the eastward energy flux at S2 peaks around one month later in Oct.. Thus a wave
energy transfer route that sequentially passes S1, S2 and S3 to influence the ATL3 region is revealed and gives the evidence
for the influence of the wave energy from off-equatorial region on the Atlantic Niño in 2019.

4   Summary

This study decomposed the wave signal from the ocean reanalysis dataset and further diagnosed equatorial waves in the
tropical Atlantic by applying a recent developed wave energy flux scheme. The equatorial waves for both climatological values
and anomalies in 2019 are detected. Strong subseasonal equatorial KW trains were revealed in 2019, which we believed to
associate with the onset of the SST event. All the first four modes are providing non-negligible contributions on the KW and
the consequent displacement of thermocline (see Figure 4), however the discrepancy of energy transfer processes among the
modes are notable. The third and fourth mode is mainly excited locally in the ATL3 region during the event while the wave
energy of the first and second mode come from the west, likely to be affected by RWs through reflections. Furthermore, in
terms of the wave travelling, owing to the relatively slow group velocity, the wave flux of the higher mode (the third and fourth
mode) is found to peak in the late Nov. and early Dec. holding the SST anomaly until the next Jan..

The extracted equatorial waves from both the climatological and the 2019 reanalysis data are demonstrating strong westward
energy flux in the off-equatorial region (especially in the first and second modes due to their short Rossby deformation radius),
which leads the wave energy to approach the western boundary for causing reflected KWs and eventually back to the equatorial
region directly or along the coastline. The ray tracing by means of Wentzel-Kramers-Brillouin (WKB) approximation had
revealed that reflected RW will transport their energy back to the equatorial region in a beta plane (Philander, 1978; Schopf
et al., 1981; Claus et al., 2014). Linear ocean model with real coastline of the Atlantic basin can further demonstrated that the
RW can be affected by the irregular African coastline to transport the energy back to the eastern Atlantic basin, but handicapped
by the radiant boundary condition, the along-shore energy fluxes off the western boundary are often missing (Kopte et al.,
2017; Song and Aiki, 2020; Kopte et al., 2018). Although previous researches based on reanalysis dataset or ocean general
circulation models (OGCM) can find general links between off-equatorial RWs and equatorial KWs by the propagation of
SLA or the advection of SST (Richter et al., 2022; Foltz and McPhaden, 2010), still no concrete evidence was found for the
baroclinic waves and their connections. This study, however, diagnosed the wave energy transfer route with reanalysis data so

as to avoid the information loss with simple linear models and illustrates the wave energy transfer process in each baroclinic modes between the equatorial and off-equatorial regions.

However, the presented diagnosis scheme has a drawback in its utilization of assumed orthogonality for linear waves in cases where nonlinearity is relatively crucial. As a result, the decomposed variability can not correctly represent the contributions of each baroclinic modes. Indeed other attempts to decompose wave-induced variability e.g. projecting the velocity and geopotentionl to eigen functions by means of the least-square method applied by Tuchen et al. (2018) may also have similar problems. Nevertheless, it is expected that the error due to nonlinearity should be controllable in the linear-dominated equatorial basins. Thus as the equatorial waves had been revealed to have great potentials in the prediction for the Atlantic Niños as well as the anomalous SST event, Benguela Niños, in the down-wave region (Bachèlery et al., 2016, 2020), we expect the rapid wave diagnosis using reanalysis data can provide a useful tool in the associated community.

Data availability. The temperature, salinity and velocity data of GLORYS12V1 product is from (https://data.marine.copernicus.eu/product/GLOBAL_MULTIYEAR_PHY_001_030/services). The OISST data used to validate the model is available via (http://apdrc.soest.hawaii.edu:80/dods/public_data/NOAA_SST/OISST/monthly).

Author contributions. Qingyang Song and Hidenori Aiki conceived the study. Qingyang Song processed the reanalysis data and performed the wave energy analysis with scientific insight of Hidenori Aiki. The paper was written by Qingyang Song with contributions of the co-author.

Competing interests. The authors declare that they have no conflicts of interest.

Acknowledgements. The authors gratefully acknowledge the financial support from the Young Scientists Fund of the National Natural Science Foundation of China (Grant Numbers 42206008) and the China Postdoctoral Science Foundation (Grant Numbers 2021M701040).

225 **References**

Aiki, H., Greatbatch, R. J., and Claus, M.: Towards a seamlessly diagnosable expression for the energy flux associated with both equatorial
and mid-latitude waves, Progress in Earth and Planetary Science, 4, 11, 2017.

Bachèlery, M.-L., Illig, S., and Dadou, I.: Forcings of nutrient, oxygen, and primary production interannual variability in the southeast
Atlantic Ocean, Geophysical Research Letters, 43, 8617–8625, 2016.

230 Bachèlery, M.-L., Illig, S., and Rouault, M.: Interannual coastal trapped waves in the Angola-Benguela upwelling system and Benguela Niño
and Niña events, Journal of Marine Systems, 203, 103 262, 2020.

Bourlès, B., Araujo, M., McPhaden, M. J., Brandt, P., Foltz, G. R., Lumpkin, R., Giordani, H., Hernandez, F., Lefèvre, N., Nobre, P., et al.:
PIRATA: A sustained observing system for tropical Atlantic climate research and forecasting, Earth and Space Science, 6, 577–616, 2019.

Carton, J. A., Cao, X., Giese, B. S., and Da Silva, A. M.: Decadal and interannual SST variability in the tropical Atlantic Ocean, Journal of
235 Physical Oceanography, 26, 1165–1175, 1996.

Claus, M., Greatbatch, R. J., and Brandt, P.: Influence of the barotropic mean flow on the width and the structure of the Atlantic equatorial
deep jets, Journal of Physical Oceanography, 44, 2485–2497, 2014.

Claus, M., Greatbatch, R. J., Brandt, P., and Toole, J. M.: Forcing of the Atlantic equatorial deep jets derived from observations, Journal of
Physical Oceanography, 46, 3549–3562, 2016.

240 Crespo, L. R., Prigent, A., Keenlyside, N., Koseki, S., Svendsen, L., Richter, I., and Sánchez-Gómez, E.: Weakening of the Atlantic Niño
variability under global warming, Nature Climate Change, 12, 822–827, 2022.

Ding, H., Keenlyside, N. S., and Latif, M.: Seasonal cycle in the upper equatorial Atlantic Ocean, Journal of Geophysical Research: Oceans,
114, 1–16, https://doi.org/10.1029/2009JC005418, 2009.

Foltz, G. R. and McPhaden, M. J.: Interaction between the Atlantic meridional and Niño modes, Geophysical Research Letters, 37, 2010.

245 Foltz, G. R., Brandt, P., Richter, I., Rodríguez-Fonseca, B., Hernandez, F., Dengler, M., Rodrigues, R. R., Schmidt, J. O., Yu, L., Lefèvre, N.,
et al.: The tropical Atlantic observing system, Frontiers in Marine Science, 6, 206, 2019.

Illig, S. and Bachèlery, M.-L.: Propagation of subseasonal equatorially-forced coastal trapped waves down to the benguela upwelling system,
Scientific reports, 9, 1–10, 2019.

Imbol Koungue, R. A., Illig, S., and Rouault, M.: Role of interannual K elvin wave propagations in the equatorial A tlantic on the A ngola B
250 enguela C urrent system, Journal of Geophysical Research: Oceans, 122, 4685–4703, 2017.

Imbol Koungue, R. A., Rouault, M., Illig, S., Brandt, P., and Jouanno, J.: Benguela Niños and Benguela Niñas in forced ocean simulation
from 1958 to 2015, Journal of Geophysical Research: Oceans, 124, 5923–5951, 2019.

Jean-Michel, L., Eric, G., Romain, B.-B., Gilles, G., Angélique, M., Marie, D., Clement, B., Mathieu, H., Olivier, L. G., Charly, R., et al.:
The Copernicus global 1/12 oceanic and sea ice GLORYS12 reanalysis, Frontiers in Earth Science, 9, 698 876, 2021.

255 Kopte, R., Brandt, P., Dengler, M., Tchipalanga, P., Macuéria, M., and Ostrowski, M.: The Angola Current: Flow and hydrographic charac-
teristics as observed at 11 S, Journal of Geophysical Research: Oceans, 122, 1177–1189, 2017.

Kopte, R., Brandt, P., Claus, M., Greatbatch, R. J., and Dengler, M.: Role of Equatorial Basin-mode resonance for the seasonal variability of
the Angola current at 11 S, Journal of Physical Oceanography, 48, 261–281, 2018.

Latif, M. and Keenlyside, N. S.: El Niño/Southern Oscillation response to global warming, Proceedings of the National Academy of Sciences,
260 106, 20 578–20 583, 2009.

Lübbecke, J. F. and McPhaden, M. J.: On the inconsistent relationship between Pacific and Atlantic Niños, Journal of Climate, 25, 4294–4303, 2012.

Matsuno, T.: Quasi-geostrophic motions in the equatorial area, Journal of the Meteorological Society of Japan. Ser. II, 44, 25–43, 1966.

265 Nnamchi, H. C., Li, J., Kucharski, F., Kang, I.-S., Keenlyside, N. S., Chang, P., and Farneti, R.: Thermodynamic controls of the Atlantic Niño, Nature communications, 6, 1–10, 2015.

Okumura, Y. and Xie, S.-P.: Interaction of the Atlantic equatorial cold tongue and the African monsoon, Journal of Climate, 17, 3589–3602, 2004.

Philander, S.: Forced oceanic waves, Reviews of Geophysics, 16, 15–46, 1978.

Richter, I., Tokinaga, H., and Okumura, Y. M.: The extraordinary equatorial Atlantic warming in late 2019, Geophysical Research Letters, 270 49, e2021GL095 918, 2022.

Rossby, C.-G.: On the propagation of frequencies and energy in certain types of oceanic and atmospheric waves, Journal of Meteorology, 2, 187–204, 1945.

Schiller, A., Wijffels, S., Sprintall, J., Molcard, R., and Oke, P. R.: Pathways of intraseasonal variability in the Indonesian Throughflow region, Dynamics of atmospheres and oceans, 50, 174–200, 2010.

275 Schopf, P. S., Anderson, D. L., and Smith, R.: Beta-dispersion of low-frequency Rossby waves, Dynamics of Atmospheres and Oceans, 5, 187–214, 1981.

Song, Q. and Aiki, H.: The Climatological Horizontal Pattern of Energy Flux in the Tropical Atlantic as Identified by a Unified Diagnosis for Rossby and Kelvin Waves, Journal of Geophysical Research: Oceans, 125, e2019JC015 407, 2020.

Song, Q. and Aiki, H.: Horizontal energy flux of wind-driven intraseasonal waves in the tropical Atlantic by a unified diagnosis, Journal of 280 Physical Oceanography, 51, 3037–3050, 2021.

Song, Q., Aiki, H., and Tang, Y.: The role of equatorially forced waves in triggering Benguela Niño/Niña as investigated by an energy flux diagnosis, Journal of Geophysical Research: Oceans, p. e2022JC019272, 2023.

Tokinaga, H. and Xie, S.-P.: Weakening of the equatorial Atlantic cold tongue over the past six decades, Nature Geoscience, 4, 222–226, 2011.

285 Toyoda, T., Nakano, H., Aiki, H., Ogata, T., Fukutomi, Y., Kanno, Y., Urakawa, L. S., Sakamoto, K., Yamanaka, G., and Nagura, M.: Energy flow diagnosis of ENSO from an ocean reanalysis, Journal of Climate, 34, 4023–4042, 2021.

Tuchen, F. P., Brandt, P., Claus, M., and Hummels, R.: Deep intraseasonal Variability in the central equatorial Atlantic, Journal of Physical Oceanography, 48, 2851–2865, 2018.

Yang, H. and Liu, Z.: Basin modes in a tropical–extratropical basin, Journal of Physical Oceanography, 33, 2751–2763, 2003.
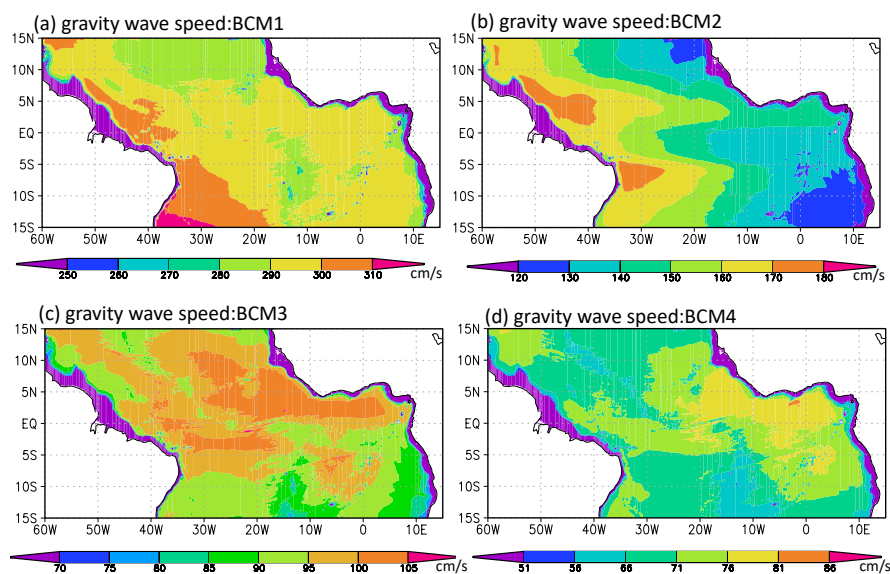
Figure 1. Gravity wave speed in the tropical Atlantic for the (a) first, (b) second, (c) third and (d) fourth baroclinic mode (BCM). The gravity wave speed is solved by Eq (1) with mean vertical profile of salinity and temperature from GLORYS12V1 product over 1993 to 2020.
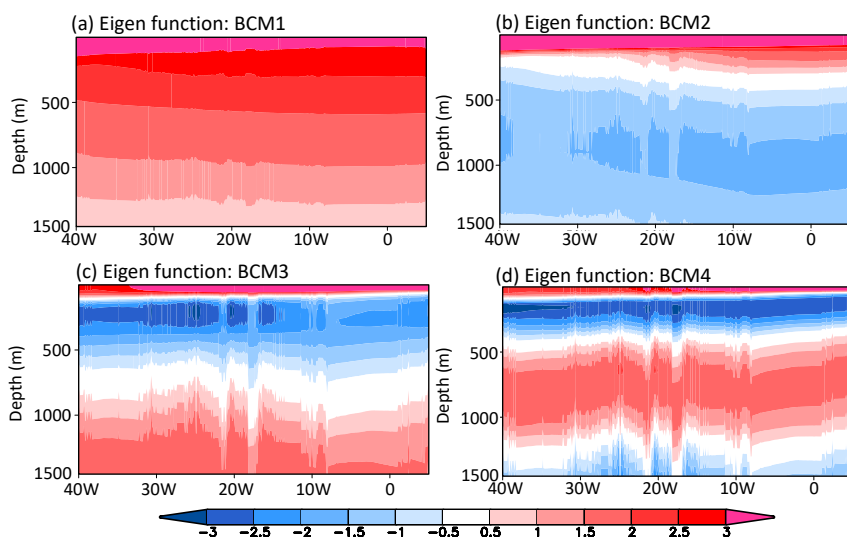
Figure 2. Eigen functions at the equator for the (a) first, (b) second, (c) third and (d) fourth baroclinic mode (BCM). The eigen function is also solved by by Eq (1) with mean vertical profile of salinity and temperature from GLORYS12V1 product over 1993 to 2020, which corresponds to the gravity wave speed (eigen value) in Figure 1.
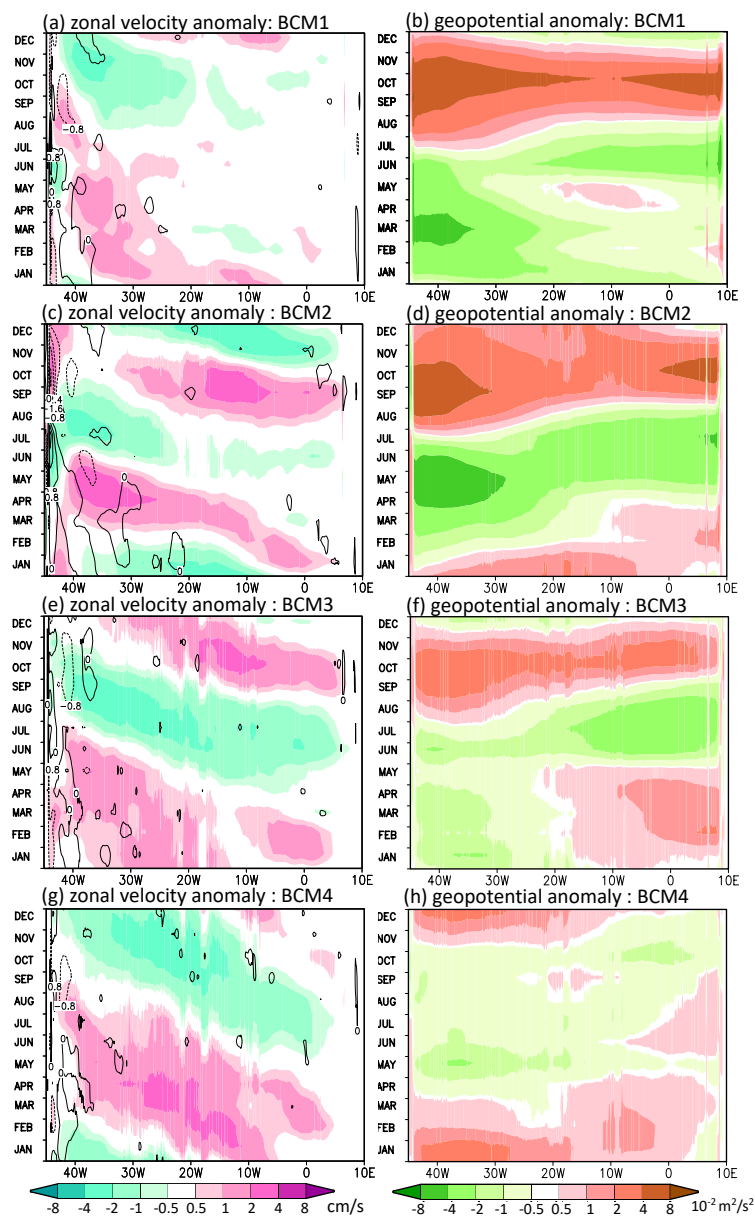
Figure 3. Hovmöller diagram for the climatology of velocity (left panels) and geopotential (right panels) at the equator decomposed from the daily GLORYS12V1 product for 2019 in the first (a,b), second (c,d), third (e,f) and fourth (g,h) baroclinic modes (BCM). Color shadings in the left panels are zonal velocity $u^{(n)}$. Contours in the left panels are meridional velocity $v^{(n)}$ with the interval of 0.8 cm/s. Color shadings in the right panels are geopotential $p^{(n)}$.
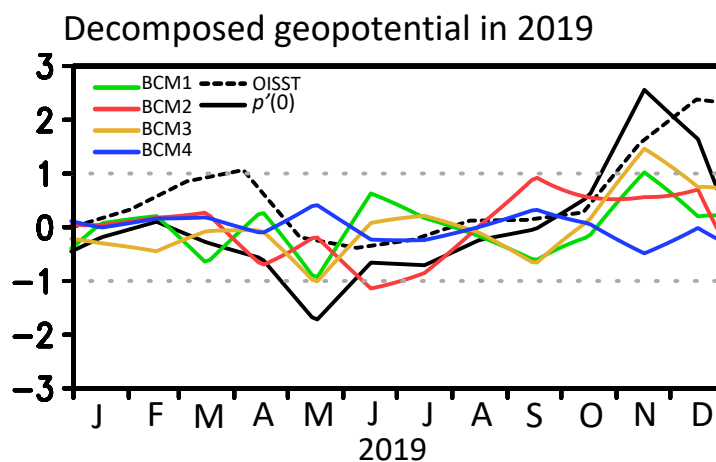
Figure 4. Timeseries of geopotential anomaly at the sea surface $p'(0)$ (solid black line), SST anomaly (dashed black line) from OI-SST (Optimum Interpolation Sea Surface Temperature) dataset and the decomposed geopotential for the first (BCM1, solid green line), second (BCM2, solid red line), third (BCM3, solid yellow line) and fourth (BCM4, solid blue line) baroclinic mode in 2019. The $p'(0)$ is calculated following Eq. (4) with the decomposed geopotential $p^{(n)}\psi^{(n)}(0)$. The anomalies of SST and geopotential are averaged over the Atlantic 3 region (ATL3, $3°$S-$3°$N,$20°$W-$0°$) and normalized by the variance of SST and $p'(0)$ respectively.
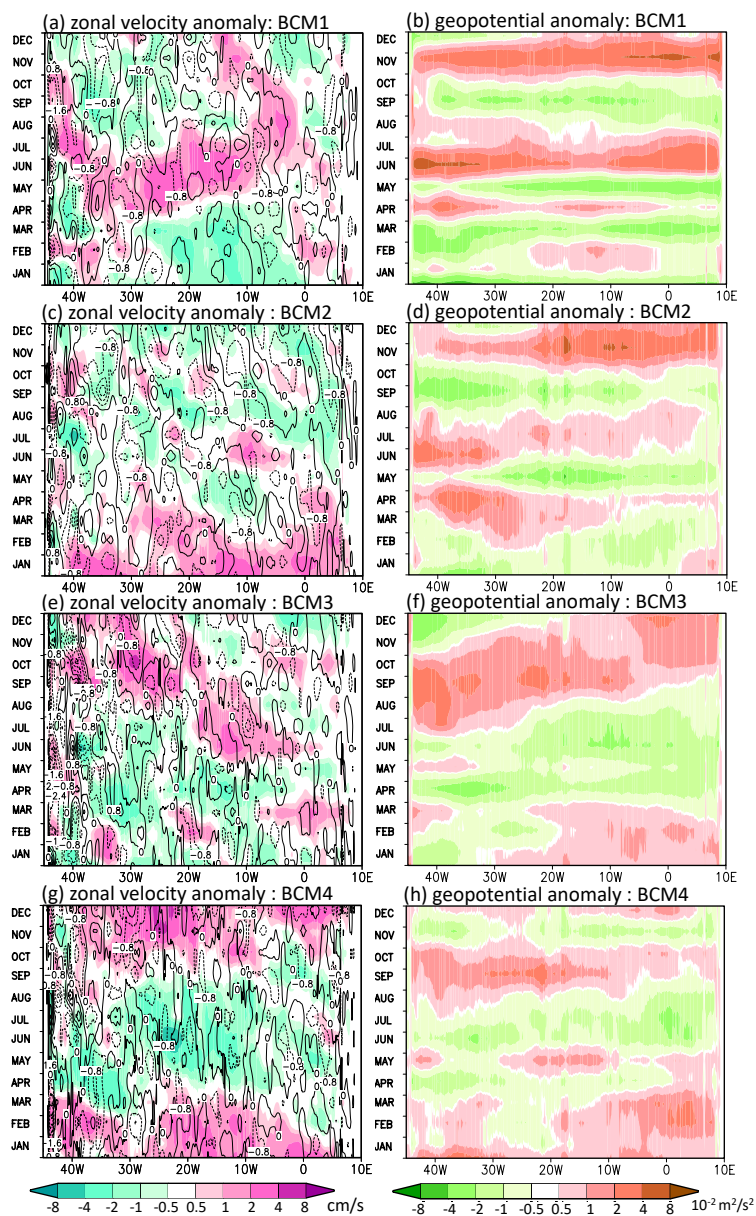
Figure 5. Same as Figure 3 but for the anomaly in the event year 2019.
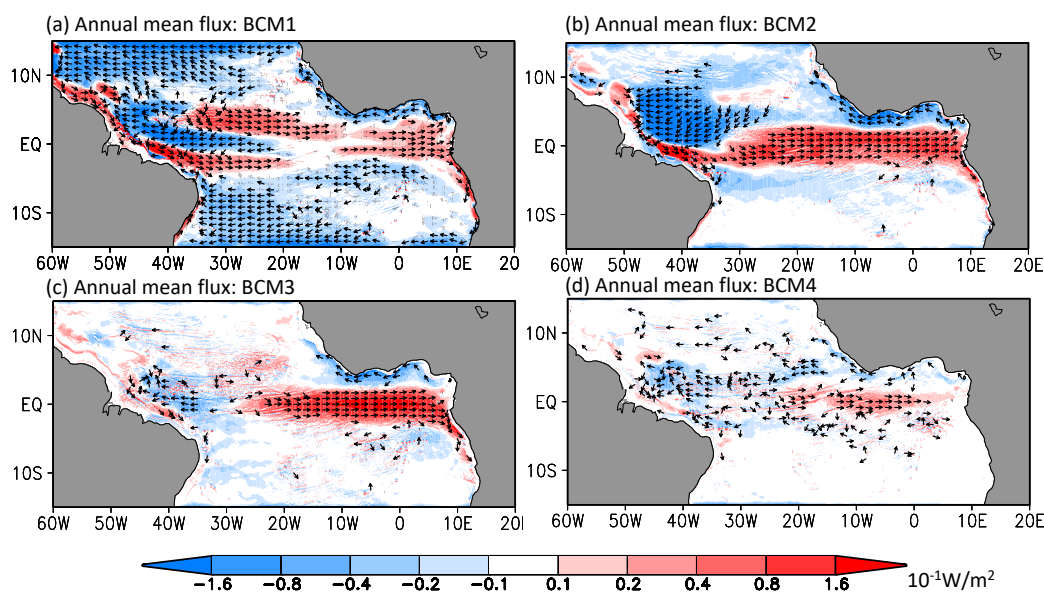
Figure 6. Annual mean climatological AGC flux for the (a) first, (b) second, (c) third and (d) fourth baroclinic modes (BCM). Color shadings: the zonal component of the AGC flux. Arrows with a constant length indicate the directions of the flux vector.
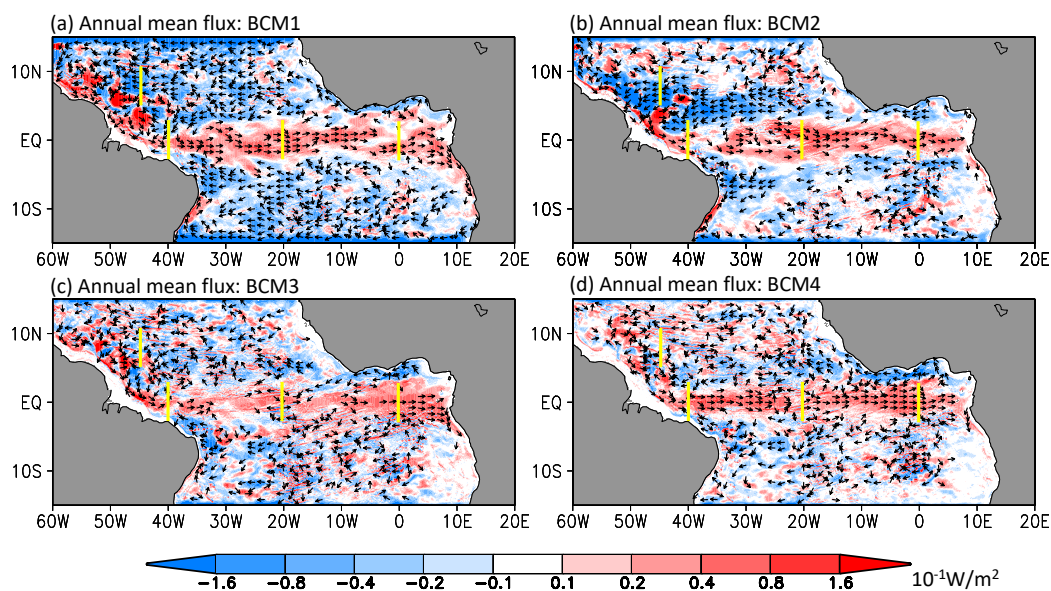
Figure 7. Same as Figure 6 but for the anomaly in 2019. Solid yellow lines indicate four meridional transections: S1 ($4°$N-$10°$N, $45°$W), S2 ($3°$S-$3°$N, $40°$W), S3 ($3°$S-$3°$N, $20°$W,) and S4 ($3°$S-$3°$N, $0°$).
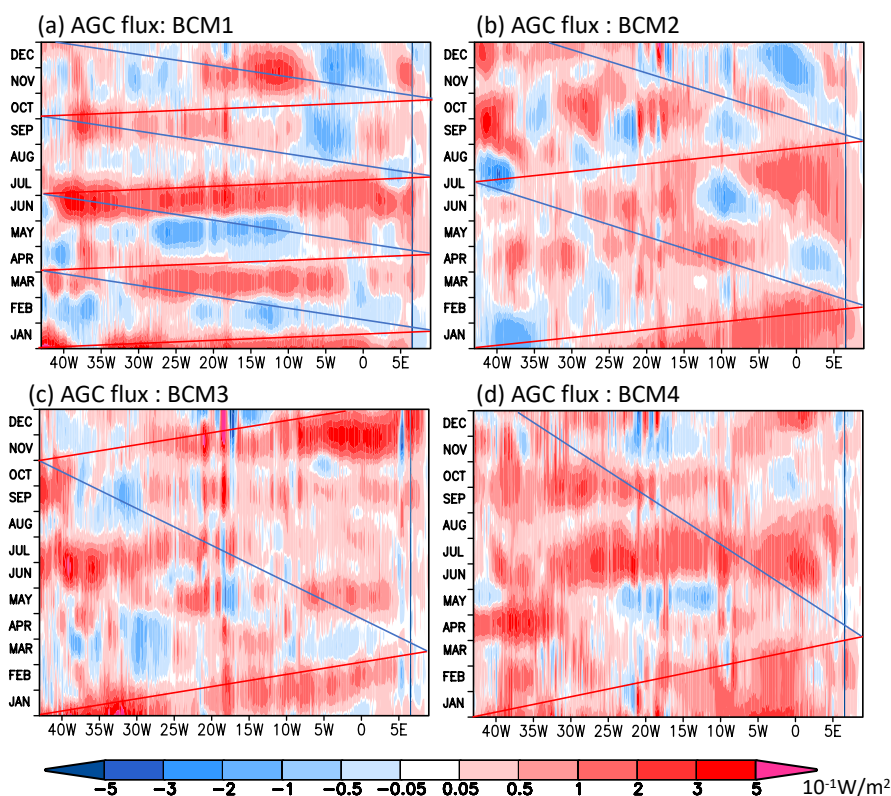
Figure 8. Hovmöller diagram for the AGC flux in 2019 at the equator in the (a) first, (b) second, (c) third and (d) fourth baroclinic modes (BCM). Color shadings are the zonal AGC flux at the equator. The solid red (blue) line represents averaged group velocity of the KW (RW) for the BCM1 of around 2.9 m/s (1.0 m/s), BCM2 of around 1.4 m/s (0.5 m/s), BCM3 of around 0.9 m/s (0.3 m/s) and BCM4 of around 0.7 m/s (0.2 m/s) at the equator (see Figure 8).
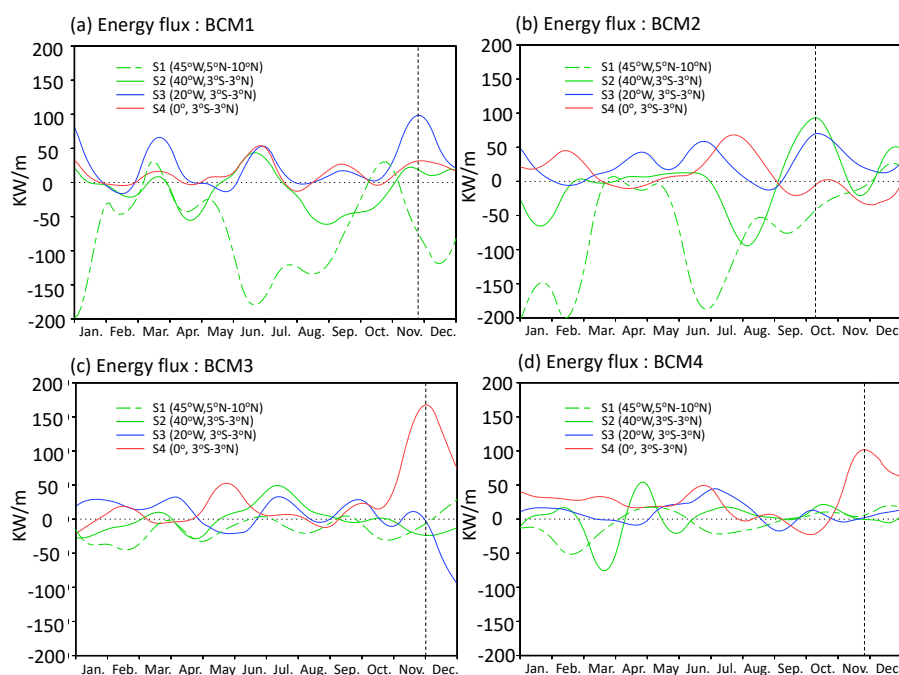
Figure 9. Time series of zonal AGC flux in 2019 for the (a) first, (b) second, (c) third and (d) fourth baroclinic modes (BCM) integrated over the transection S1 (dashed green line), S2 (solid green line), S3 (solid blue line) and S4 (solid red line). Dotted black lines indicate the peaks of the positive zonal flux passing the four sections in 2019.